Designed Polyelectrolyte Shell on Magnetite Nanocore for Dilution-Resistant Biocompatible Magnetic Fluids

ARTICLE *in* LANGMUIR · NOVEMBER 2012

Impact Factor: 4.46 · DOI: 10.1021/la302660p · Source: PubMed

7 AUTHORS, INCLUDING:

Erzsébet Illés
Vinča Institute of Nuclear Sciences
34 PUBLICATIONS **1,067** CITATIONS
SEE PROFILE

Marta Szekeres
University of Szeged
43 PUBLICATIONS **1,216** CITATIONS
SEE PROFILE

Istvan Zupko
University of Szeged
170 PUBLICATIONS **1,545** CITATIONS
SEE PROFILE

Etelka Tombácz
University of Szeged
131 PUBLICATIONS **3,394** CITATIONS
SEE PROFILE

Langmuir

Article

pubs.acs.org/Langmuir

Designed Polyelectrolyte Shell on Magnetite Nanocore for Dilution-Resistant Biocompatible Magnetic Fluids

Ildikó Y. Tóth,[†] Erzsébet Illés,[†] Rita A. Bauer,[†,§] Dániel Nesztor,[†] Márta Szekeres,*[,†] István Zupkó,[‡] and Etelka Tombácz*[,†]

[†]Department of Physical Chemistry and Materials Science, University of Szeged, Aradi Vt. 1, H-6720 Szeged, Hungary

[‡]Department of Pharmacodynamics and Biopharmacy, University of Szeged, Eötvös u. 1, H-6720 Szeged, Hungary

ABSTRACT: Magnetite nanoparticles (MNPs) coated with poly(acrylic acid-*co*-maleic acid) polyelectrolyte (PAM) have been prepared with the aim of improving colloidal stability of core−shell nanoparticles for biomedical applications and enhancing the durability of the coating shells. FTIR-ATR measurements reveal two types of interaction of PAM with MNPs: hydrogen bonding and inner-sphere metal−carboxylate complex formation. The mechanism of the latter is ligand exchange between uncharged −OH groups of the surface and $-COO^-$ anionic moieties of the polyelectrolyte as revealed by adsorption and electrokinetic experiments. The aqueous dispersion of PAM@MNP particles (magnetic fluids − MFs) tolerates physiological salt concentration at composition corresponding to the plateau of the high-affinity adsorption isotherm. The plateau is reached at small amount of added PAM and at low concentration of nonadsorbed PAM, making PAM highly efficient for coating MNPs. The adsorbed PAM layer is not desorbed during dilution. The performance of the PAM shell is superior to that of poly(acrylic acid) (PAA), often used in biocompatible MFs. This is explained by the different adsorption mechanisms; metal−carboxylate cannot form in the case of PAA. Molecular-level understanding of the protective shell formation on MNPs presented here improves fundamentally the colloidal techniques used in core−shell nanoparticle production for nanotechnology applications.

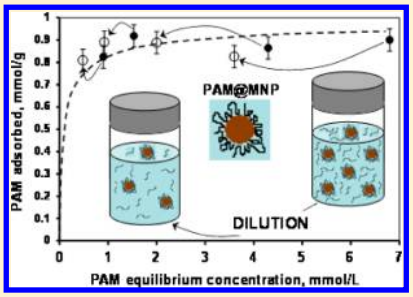

INTRODUCTION

The preparation of magnetite nanoparticles (MNPs) for application both in diagnostics and in therapy has been the focus of theranostics for the last several decades.[1−12] Despite the very intense research, only few formulations are currently available for clinical application in MRI, drug delivery, controlled drug release, or magnetic hyperthermia.[13−15] The magnetic properties and biocompatibility of MNPs make them a powerful competitor of other contrast agents (e.g., the widely used gadolinium complexes), the cytotoxicity and organ-specific side effects of which have raised some concern.[16−18] The nanoparticles must be coated to prevent dissolution and aggregation of MNPs under physiological conditions (i.e., neutral pH and high salt concentration), to protect against protein adsorption (with subsequent denaturation), and to introduce anchoring sites for drug attachment. One of the promising techniques to cover particle surface is the adsorption of biocompatible hydrocolloids: uncharged polymers and polyelectrolytes (PEs).[19] Detailed studies of the mechanism of adsorption of PEs are relatively rare in the literature, mainly because of its complex character, although the knowledge of the basic processes is invaluable in the development of functional nanocomposites for biomedical applications.[20]

Macromolecules can act both as dispersants and as flocculants depending on their chemical structure, molecular weight, adsorbed amount, as well as on their physicochemical properties in solution and at the solid/liquid interface. Lyklema and Deschenes[21] discuss in detail the chemical and electrostatic aspects of polyelectrolyte adsorption and provide a comprehensive review of the topic. They emphasize that the primary factor in PE adsorption is specific (non-Coulombic) interaction, in contrast to the widely accepted and apparently evident expectation that the main driving force should be of electrostatic origin. Specific interactions are so effective that the adsorbed layer of the polyelectrolyte easily overcompensates the charge of the adsorbent and stabilizes the particles electrosterically. High overcharging demonstrates clearly that specific (non-Coulombic) interactions can lead to adsorption even against electrostatic repulsion. Electrostatic and specific adsorption can be distinguished by studying the effect of ionic strength and the shape of the adsorption isotherms. The ionic strength of the medium influences electrostatic adsorption, but has a minor effect on specific adsorption. The shape of the isotherm is of H (high-affinity)-type for mainly specific adsorption,[22,23] but increased involvement of electrostatic interactions gradually transforms it to L (Langmuir)-type. High-affinity adsorption is marked as "irreversible", if the adsorbed layer cannot be detached by washing during the time of the experiment. Typical specific (nonelectrostatic) interactions are listed generally as van der Waals attraction, H-bond formation, hydrophobic effect (depletion of hydrophobes from aqueous medium), ion-pair formation, complex (coordinative),

Received: July 3, 2012
Revised: October 9, 2012
Published: November 9, 2012

   dx.doi.org/10.1021/la302660p | *Langmuir* 2012, 28, 16638−16646

and covalent bond formation. In case of adsorption of carboxylic polyelectrolytes on metal oxide surfaces, the possibility of complex formation between the carboxylic moieties and the metal ions is considered in many publications.[24−28]

Our aim was to fasten a PE layer to the surface of MNPs so strongly that besides rendering the magnetite nanoparticles colloidally stable at physiological pH and salt concentrations, the coating PE shell resists dilution as well; that is, the PE molecules are not desorbed during dilution. Soenen et al.[29] have given experimental evidence of the effect of the coating shell on the stability of MNPs in cellular environment: citric acid-coated MNPs degraded quickly; dextran-coating led to increased stability; however, magnetoliposomes proved to be the most stable. Chemical reactions are frequently involved in the surface modification of MNPs, to achieve acceptable dilution stability.[30−34] The disadvantages of this approach are that the reaction conditions are generally harsh, the reactants are not necessarily biocompatible, and unwanted byproducts can appear. To overcome these drawbacks, we use mild colloidal methods to prepare biocompatible aqueous MFs and to localize carboxylate groups on the surface of MNPs for later attachment of biomedical functionality. In our previous work, the mechanism of MNP coating via adsorption of poly(acrylic acid) (PAA) has been studied in detail.[35] The salt resistance of the particles satisfied the physiological requirement, but only at a large excess of PAA relative to the plateau of the adsorption isotherm. In the present study, we have chosen poly(acrylic acid-*co*-maleic acid) copolymer (PAM) for coating the MNPs. We presumed that the PAM layer can be fastened stronger to iron oxide particles than can the PAA layer, because of the known propensity of maleic acid to form metal−carboxylate complexes both in solution and at oxide/electrolyte interfaces.[36−39] Future biomedical application of the PAM-coated MNPs (PAM@MNPs) requires biocompatible particles, and so we performed in vitro biocompatibility tests as well.

MATERIALS AND METHODS

Magnetite (Fe_3O_4) nanoparticles (MNPs) were prepared via alkaline hydrolysis of a mixture of iron(II) and iron(III) chloride. The procedure is described in detail in our previous publications.[40−42] The degree of monodispersity of the particles was relatively high according to transmission electron micrographs (not shown here), and the average particle size was ∼8 nm.

Poly(acrylic acid-*co*-maleic acid) (PAM) (Sigma-Aldrich, average $M_w \approx 3000$ Da) was used without further purification. PAM is a weak polyelectrolyte with pH-dependent degree of dissociation. The notation PAM is used in this Article regardless of the actual degree of dissociation of the carboxylic groups, $\alpha = [-COO^-]/([-COO^-] + [-COOH])$. The amount of PAM is expressed through the number of moles of dissociable groups. The acrylic acid-*co*-maleic acid repeating units (M_w = 188 g/mol) contain three dissociable groups, the specific amount of which is 3/188 = 0.0159 mol/g.

HCl, NaOH, and NaCl solutions were used to adjust the pH and salt concentration in all experiments. All of these reagents were of analytical grade, obtained from Molar (Hungary). Ultrapure water from a Milli-Q RG water purification system (Millipore) was used in all experiments. All measurements were performed at 25 ± 1 °C. The results represent the mean values of measured data accumulated in n experiments (or samplings). The values of standard deviation ($SD_{(n-1)}$) are calculated by the unbiased method. The values and origin of n vary with the experimental methods as given below.

Acid−Base Titrations. Potentiometric acid−base titrations have been performed according to the procedure described previously.[43] The background electrolyte NaCl was indifferent with no specific interactions of its ions with either MNP or PAM. The data points of the titration results express equilibrium states. The equilibrium criterion of ΔpH/min < 0.01 was used.

Adsorption and Desorption Experiments. The adsorption isotherm of PAM at the MNP surface was determined at pH = 6.5 ± 0.3 and I = 0.01 M. We have used the batch method, similarly to humic acid, citric acid, or poly(acrylic acid) adsorption described in our previous publications.[35,44,45] The MNPs were equilibrated for 24 h with PAM solutions of concentration between 0.5 and 15 mM at a solid/liquid ratio of 20 g/L. The pH was set at the start of the adsorption and readjusted if necessary. The solid phase was separated by centrifuging at 14 000 rpm for 1 h. Nonsettling dispersions were coagulated by a droplet of 1 M NaCl solution and centrifuged additionally for 1 h. Alternatively, the separation of highly stable dispersions was assisted by a permanent magnet. The equilibrium concentration of the supernatants was determined by measuring the absorbance at 223 nm in a USB4000 spectrometer (Ocean Optics). The baseline of the absorption spectra increased systematically with increasing PAM concentrations. The latter effect is due to the appearance of Fe^{3+} traces, according to the test of Fe^{3+} addition in separate PAM calibration series. Thus, the absorbance of the supernatants at 250 nm was subtracted from the spectra to correct for the baseline shift. The adsorbed amount of PAM (n^{σ}_{PAM}) was calculated using the material balance equation for adsorption, $n^{\sigma}_{PAM} = (V/m)\cdot\Delta c_{PAM}$, where V/m is the solution/adsorbent phase ratio (L/g) and Δc_{PAM} is the change in the polyelectrolyte concentration in the aqueous phase due to the adsorption (mol/L). The adsorption isotherm was plotted as the function of the equilibrium PAM concentration. The desorption experiments have been performed by diluting four selected dispersions of the adsorption series with 0.01 M NaCl solution at pH ≈ 6.5, after 24 h of adsorption equilibration. The factor of dilution was 2. The samples were left for 24 h before measuring the new equilibrium concentration by using the same method as in the adsorption experiments. The $SD_{(n-1)}$ is calculated for n = 9 (three separate determinations of equilibrium PAM concentration in three parallel experiments).

FTIR-ATR Measurements. FTIR-ATR spectra were recorded with a Bio-Rad Digilab Division FTS-65A/896 spectrometer (with DTGS detector), using a Harrick's Meridian Split Pea Diamond ATR accessory. The absorbance of the samples was measured in single reflection mode over the 400−4000 cm^{-1} range (with resolution of 2 cm^{-1}), accumulating 256 scans. Magnetite suspensions, PAM solutions, or PAM@MNP composite suspensions were dried on the crystal surface. For FTIR experiments, the amount of added PAM@MNP was 1.2 mmol/g. The background spectra were measured on clean and dry diamond crystal.

Electrokinetic Potential Measurements. Electrophoretic mobilities of the pure magnetite and PAM@MNP dispersions were measured in a Zetasizer Nano ZS (Malvern) dynamic light scattering (DLS) apparatus with a 4 mW He−Ne laser source (λ = 633 nm), using disposable zeta cells (DTS 1060). The instrument was calibrated by measuring the zeta potential of a zeta-standard (55 ± 5 mV) supplied by Malvern. The accuracy of the measurements is ±5 mV as reported by Malvern. The concentration of the dispersions was set to give optimal intensity of ∼10^5 counts per second. After preparation, the samples were left standing for 1 day. Prior to the measurements, the samples were agitated with ultrasound for 10 s and allowed to relax for 2 min. The effect of PAM addition on the electrophoretic mobility of the MNPs was measured at pH = 6.5 ± 0.3 and 0.01 M ionic strength. The effect of pH variation (between 3 and 10) was measured on the uncoated and on three coated MNPs (i.e., at 0, 0.1, 0.47, and 1.3 mmol/g of added PAM) at 0.01 M ionic strength. The Smoluchowski equation was applied to convert the electrophoretic mobilities to electrokinetic potential values. The $SD_{(n-1)}$ of the electrokinetic measurements is calculated for n = 36 (three separate sample dispersions, 12 samplings for each).

Particle Size Determination. DLS measurements of average particle diameter were performed using a Zetasizer Nano ZS apparatus (Malvern) operating in backscattering mode at an angle of 173°. The added amounts of PAM, the pH range, and the ionic strength were

dx.doi.org/10.1021/la302660p | Langmuir 2012, 28, 16638−16646

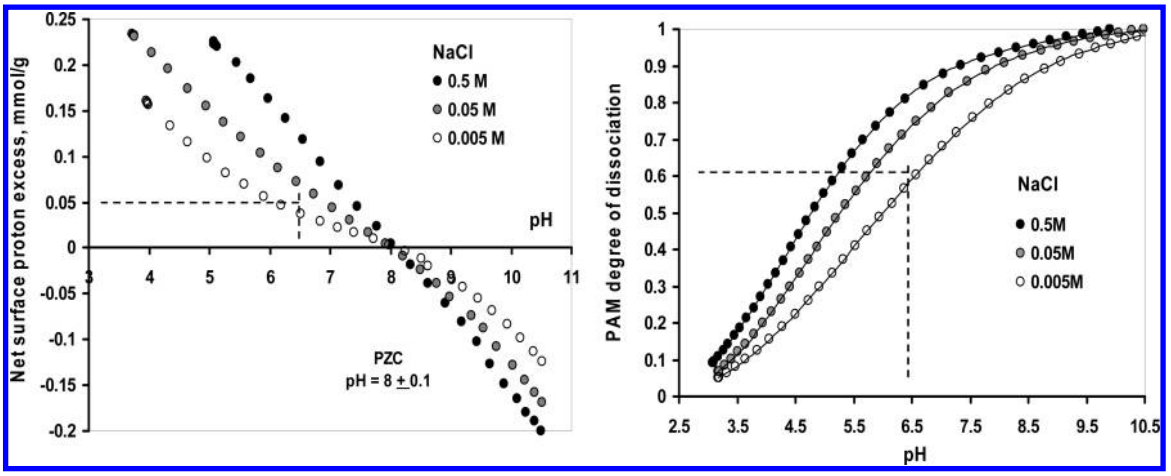

Figure 1. pH- and ionic strength-dependent charging of MNP (left side) and PAM (right side). Note that the surface charge density of MNPs is proportional to the measured net surface proton excess (see in the text). The dashed lines are the projections of net surface proton excess and degree of dissociation, respectively, at pH ≈ 6.5 and at I ≈ 0.01 M, the conditions of PAM@MNP preparation.

identical to those in the electrokinetic experiments. The intensity average values (Z_{ave}), chosen to characterize the size of the particles or aggregates, represent the hydrodynamic diameters. We used the second- or third-order cumulant fit of the autocorrelation functions, depending on the degree of polydispersity. The $SD_{(n-1)}$ of the Z_{ave} values is calculated for n = 30 (three separate sample dispersions, 10 samplings for each).

Coagulation Kinetics. The effect of adsorbed PAM on the colloidal stability of magnetite nanoparticles was tested in coagulation kinetics experiments at different NaCl concentrations at pH = 6.5 ± 0.3. We measured the change in Z_{ave} with time by using a Nano ZS apparatus (Malvern). In a typical experiment, data were collected for 15 min with a time resolution of 60 s. Plots of the stability ratio (log W) as a function of the electrolyte concentration (log c_{NaCl}) were used to determine the critical coagulation concentration (CCC), which characterizes the salt tolerance of the uncoated and coated MNPs. W is the ratio of the initial slope of the kinetic curve measured at the fast coagulation rate $dZ_{ave}/dt = f(t)_{fast}$ to that of actual (fast or slow) coagulation.[40,46−48] The $SD_{(n-1)}$ for the Z_{ave} values is calculated with n = 3 (three separate sample dispersions).

Because the majority of experiments were performed at pH = 6.5 ± 0.3 and I = 0.01 M, we simplify the notion of this pH value as pH ≈ 6.5 and omit noting pH and ionic strength unless it has special significance or the values are different.

Biocompatibility Tests. The influence of the PAM@MNPs on the colloidal state of whole blood of healthy volunteers was assessed by erythrocyte sedimentation rate (ESR) experiments, using a Sedi-15 automated blood sedimentation instrument (BD Inc., U.S.) and Seditainer 1.8 vacutainer tubes (BD Inc., U.S.). The experiments test the change in the stability of the suspended red blood cells (RBC) in plasma under specified conditions.[49] We used the Westergren[50] method; that is, we observed the level to which the sharp boundary of the settling RBCs falls in 1 h time, leaving plasma as clear supernatant. Well-stabilized red blood cells of healthy donors settle with ESR < 20 mm/h. An increase in the ESR value reveals RBC coagulation, which can be caused by any effect that shields the negative charges stabilizing the RBCs electrostatically. Biocompatible additives are not expected to induce RBC coagulation. PAM@MNP dispersions (pH ≈ 6.5, I = 0.01 M) were added to citrate-anticoagulated blood samples of three healthy donors (no. 1−no. 3). The PAM@MNP dispersion with 1.2 mmol/g added PAM was used, and magnetite concentrations in the loaded blood samples were 0.033, 0.066, and 0.16 mg/mL. Reference blood samples (without magnetite addition) were diluted with 0.01 M NaCl solution of pH ≈ 6.5 to the same degree as the MNP-loaded samples. The accuracy of the ESR measurements is ±3 mm/h as given in the manual of Sedi-15.

Human cancer cell lines (A431, A2780, and MCF-7 isolated from skin, ovary, and breast carcinomas, respectively) were maintained in minimal essential medium supplemented with 10% fetal bovine serum (FBS) and 1% nonessential amino acids and an antibiotic-antimycotic mixture (AAM). The cells were grown in a humidified atmosphere of 5% CO_2 at 37 °C. All cell lines were purchased from the European Collection of Cell Cultures (Salisbury, UK). Cells were seeded onto 96-well plates at a density of 5000 cells/well and allowed to stand overnight, after which the medium containing the tested agent (PAM@MNP suspension) was added. Final PAM@MNP concentration in the samples varied between 0.001 and 0.1 mg/mL. After a 72 h incubation period, viability was determined by the addition of 20 μL of MTT ([3-(4,5-dimethylthiazol-2-yl)-2,5-diphenyltetrazolium bromide]) solution (5 mg/mL). The precipitated formazan crystals were solubilized in DMSO (100 μL), and the absorbance was read at 545 nm with an ELISA reader.[51] The experiments were performed with five parallel wells.

RESULTS AND DISCUSSION

Charging of MNP and PAM. The pH- and ionic strength-dependent charging of MNP and PAM is seen in Figure 1, as obtained from potentiometric acid−base titrations. The primary result of titrations is the sum of proton consumption in all probable processes such as dissolution or hydrolysis, for example, occurring in parallel with surface charging. However, only protonation or deprotonation of the ionizable groups of solid surface (≡Fe−OH + H^+ ↔ ≡Fe−OH_2^+ or ≡Fe−OH ↔ ≡Fe−O^- + H^+) and polyelectrolyte (−COOH ↔ −COO^- + H^+) can produce intrinsic charge on pure materials. Thus, the conditions of the titration must ensure that (i) surface charge forms exclusively via protonation/deprotonation of ionizable groups, (ii) additional processes with proton participation are excluded, and (iii) the background electrolyte is indifferent.[52,53] Under these conditions, the primary results of titrations (i.e., the net proton consumption) represent net surface proton excess values that can be converted to surface charge density data. Our titration procedure fulfills the above conditions,[43] and we obtain the direct values of net surface proton excess and degree of dissociation that correctly represent the pH-dependent charging of interacting partners.

The surface of MNPs is uncharged at the pH of the point of zero charge (PZC) at pH = 8 ± 0.1, and it is positively or negatively charged below or above it, respectively. PAM can only gain negative charges. The titration results of PAM are very similar to those of PAA.[35] The dashed lines in Figure 1 show the charge state of MNP and PAM at the pH and ionic

dx.doi.org/10.1021/la302660p | Langmuir 2012, 28, 16638−16646

strength of the PAM@MNP preparation (pH ≈ 6.5 and I = 0.01 M), chosen to ensure optimal adsorption of PAM at MNP surface, that is, formation of thick and dense adsorbed layer for efficient electrosteric stabilization. On the basis of the general principles of polyelectrolyte adsorption,[21] both MNP and PAM should be moderately charged, and it is preferable that the charges have opposite sign. From the titration results, such an optimum charge state is found at pH ≈ 6.5 and I ≈ 0.01 M, where the positive charge density of MNP is ∼0.05 mmol/g, and the degree of dissociation of the anionic PAM is ∼0.6.

Adsorption of PAM on MNP. The adsorption isotherm of PAM on the MNP is presented in Figure 2, in parallel with that of PAA.[35] PAM has an H-type isotherm with high-affinity limit of adsorption at ∼0.3 mmol/g (much above the amount of the positive charge on MNP ∼0.05 mmol/g), followed by a reversible part until the plateau is reached at ∼0.9 mmol/g. The same high-affinity limit of ∼0.3 mmol (−COOH)/g was found for citric acid adsorption in our earlier work,[44] indicating a similar mechanism of both small molecular CA and macromolecular PAM adsorption. Each monomer unit (acrylic-*co*-maleic acid) of PAM has three carboxylic groups, two of which belong to maleic acid and are capable of complex formation,[36,37,39] similarly to the well-known metal−citrate complexation.[54,55] The adsorption isotherm of PAA has completely different shape:[35] the high-affinity part is missing and the plateau is much lower (∼0.6 mmol/g).

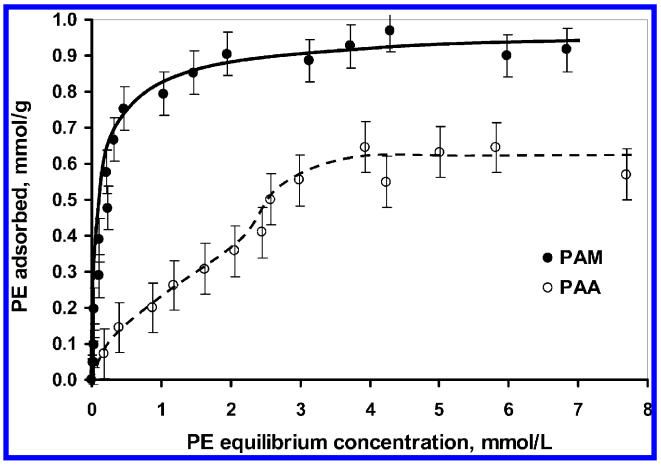

Figure 2. Adsorption isotherms ($SD_{(n-1)}$ = 0.12) of polyelectrolytes (PE) PAM and PAA on the MNPs at pH ≈ 6.5 and I = 0.01 M. Lines are drawn as a guide for the eye.

FTIR-ATR Analysis of Adsorption. Figure 3 shows the IR absorption spectra of pure MNP, PAM, and PAM-coated MNP. The characteristic bands of protonated (acidic) carboxyl groups are the C=O stretching band around 1700 cm^{-1} ($\nu_{C=O}$) and the C−OH stretching/bending vibrations between 1200 and 1300 cm^{-1} (ν_{COH}). The deprotonated carboxylates provide the asymmetric and symmetric vibrations of COO^- around 1600 cm^{-1} ($\nu_{COO-,as}$) and 1400 cm^{-1} ($\nu_{COO-,sym}$). In the spectrum of PAM (Figure 3, left side), $\nu_{C=O}$ = 1697 cm^{-1} is present as a shoulder, but in the PAM@MNP spectrum, it is shifted and forms a definite band at 1720 cm^{-1} due to the adsorption. The ν_{COH} ≈ 1200 cm^{-1} vibration is seen as a step in the spectrum of PAM, and its intensity increases slightly due to the adsorption. These observations suggest that the protonated carboxyls are involved in the adsorption of PAM. The increase in the relative intensities may be connected with an increase in the amount of protonated carboxyls at the surface as compared to the dissolved state. The latter can be explained by the mechanism of proton transfer from surface $\equiv Fe-OH_2^+$ groups to the originally dissociated $-COO^-$ groups of PAM, as discussed earlier.[35] The positions of the asymmetric and symmetric carboxylate bands change definitely due to the adsorption: $\nu_{COO-,as}$ shifts from 1571 to 1578 cm^{-1} and $\nu_{COO-,sym}$ shifts from 1404 to 1408 cm^{-1}, indicating the formation of direct metal−carboxylate complexes.[56] The shift of the $\nu_{COO-,as}$ and $\nu_{COO-,sym}$ bands was not observed in the adsorption of PAA, showing the absence of direct Fe−carboxylate complex formation.[35] Thus, the IR spectroscopy results allow us to make a clear distinction between the adsorption mechanisms of PAM and PAA. The presence of surface Fe−carboxylate complex bonds explains the strong chemical binding of PAM and the high-affinity adsorption isotherm. On the other hand, the absence of surface complexation is responsible for the L-type isotherm of PAA (Figure 1). The chemical structures of PAM and PAA are very similar, yet PAA is not capable of Fe−carboxylate formation on MNP's surface. It is apparent that the biacidic character of carboxylates is necessary for complex formation. This observation is in contrast with some literature data, according to which both PAA and bicarboxylic PEs form metal−carboxylate complexes with various metal oxides.[6,7,24,25,28]

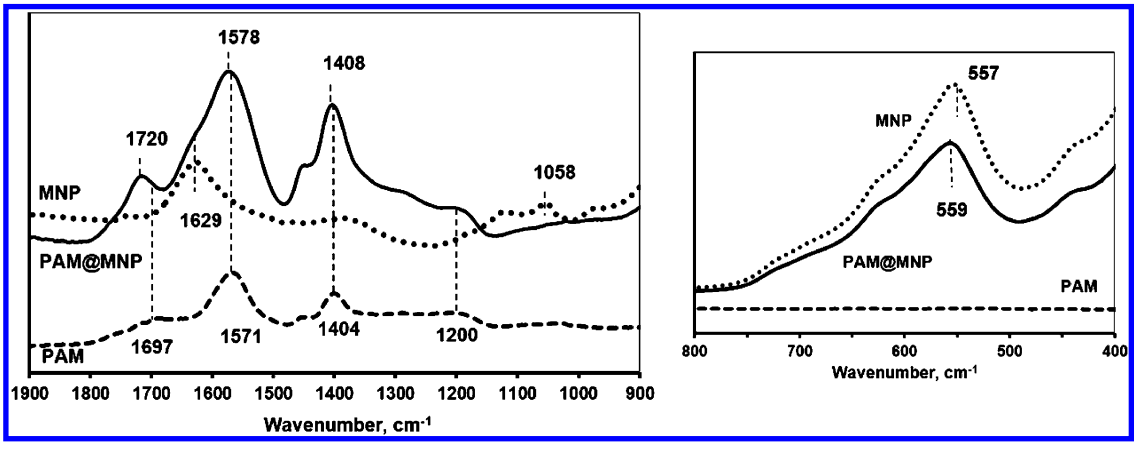

Figure 3. FTIR-ATR absorption spectra (arbitrary units) of PAM, magnetite (MNP), and PAM-coated magnetite (PAM@MNP) in the 900−1900 cm^{-1} (left side) and in the 400−800 cm^{-1} (right side) range. Samples were dried on the diamond crystal from solutions/dispersions at pH ≈ 6.5.

dx.doi.org/10.1021/la302660p | *Langmuir* 2012, 28, 16638−16646

The two characteristic bands of the surface −OH groups of MNPs (OH-deformation band at ν = 1058 cm^{-1} and H-bonded OH-stretching[57] at ν = 1629 cm^{-1}) vanish from the spectrum due to PAM adsorption, indicating that direct Fe−carboxylate complexation can occur through the ligand exchange reaction:

$$\equiv Fe - OH + R - COO^- \rightarrow Fe - OOC - R + OH^- \quad (1)$$

Some of the negative charges of PAM become neutralized in this reaction, while the charge of the MNP does not change. On the contrary, the 1058 and 1629 cm^{-1} Fe−OH bands did not vanish during adsorption of PAA,[35] which again reflects the absence of metal−carboxylate complexation. The Fe−O band[58] of MNP at 557 cm^{-1} shifts to slightly higher wavelength upon PAM adsorption (Figure 3, right side). A similar observation was made for PAA adsorption.[35]

Electrokinetic Potential, Particle Size, and Aggregation. The changes in the electrokinetic potential and the adsorbed amount are plotted in Figure 4 as a function of PAM addition. The isoelectric point (IEP, the pH at which MNP carries no net electrophoretic charge) is at 0.17 mmol/g of added PAM. This is lower than the high-affinity adsorption limit (~0.3 mmol/g in Figure 2), and so practically all added PAM is adsorbed. Considering that ~60% of the 0.17 mmol/g of PAM is dissociated (Figure 1, right side), the total amount of adsorbed carboxylate groups at the IEP is ~0.1 mmol/g. This amount of negative charge clearly overcompensates the original positive charge of the MNPs of ~0.05 mmol/g (Figure 1, left side). However, the condition of electroneutrality at the IEP dictates that the excess negative charge introduced by PAM adsorption is neutralized in some way. Indeed, FTIR spectra showed the formation of direct metal−carboxylate bonds via the ligand exchange reaction (eq 1), neutralizing carboxylates, but not changing the surface charge of MNP. As a contrast, the charge of MNP was compensated almost quantitatively at the IEP in PAA adsorption,[35] and in line with this, we have not found signs of metal−carboxylate complex formation in the IR spectra of PAA@MNP. At ~0.4 mmol/g of PAM addition, the particles become fully dispersed (see the pictures inserted in Figure 4), which is supported by the large absolute values of the electrokinetic potential, −40 mV. At higher added amounts of the anionic PAM, the electrokinetic potentials remain unchanged, but the adsorbed amounts increase to ~0.9 mmol/g.

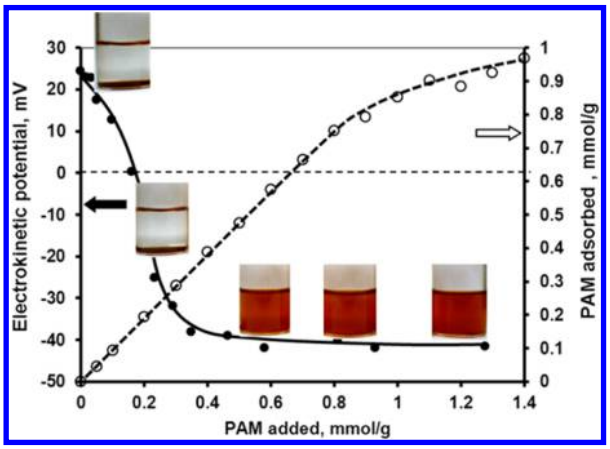

Figure 4. Effect of PAM addition on the charge state of MNPs and the colloidal stability of the dispersions (pH ≈ 6.5 and I = 0.01 M). The adsorption ($SD_{(n-1)}$ = 0.12) and the electrokinetic potential ($SD_{(n-1)}$ = 1) data are shown. For the sake of clarity, the error bars are omitted. Lines are drawn as guides for the eye.

At the plateau of the adsorption isotherm (0.9 mmol/g of adsorbed amount), the ratio between the calculated area of MNP occupied by an AM repeating unit and the area demand of AM is 1.08. For comparison, the same adsorption density for the PAA adsorption at the plateau of the adsorption isotherm (0.6 mmol/g) is 0.47. Thus, at the respective plateau values of the adsorption, the surface coverage of PAA is one-half of that of PAM. Consequently, PAA only decorates the nanoparticle surface, while the PAM coverage is full. In the above calculations, the approximate area demand of the repeating units, AM 0.6 nm^2 and AA 0.13 nm^2, and the measured specific surface area of the MNP, 100 m^2/g,[40] were used.

Figure 5 shows the changes in pH-dependent colloidal stability of MNPs with increasing amounts of added PAM. Without PAM, reasonable colloidal stability can only be observed at pH values below 5 or above 10, seen as the

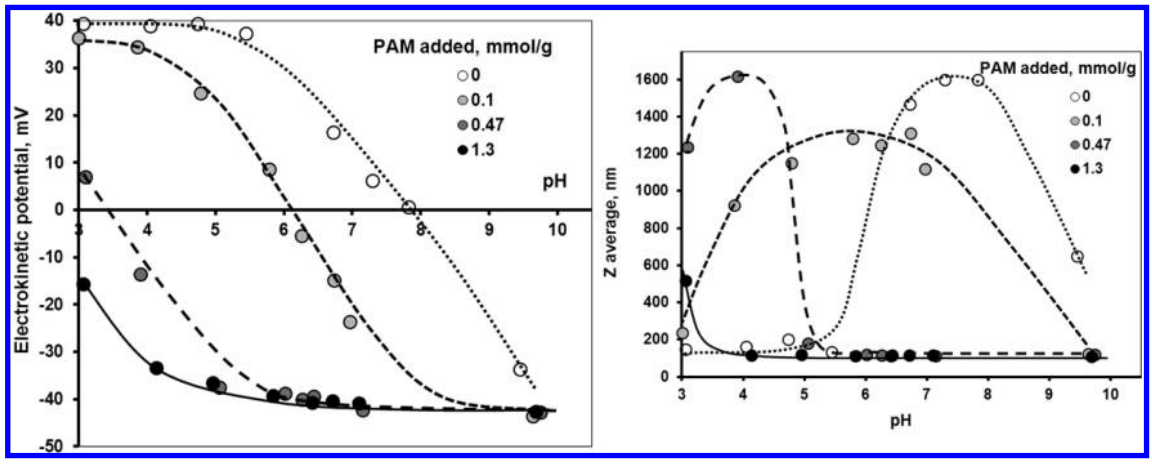

Figure 5. pH-dependent electrokinetic potential (left side) and particle diameter (right side) of MNPs at PAM loadings of 0, 0.1, 0.47, and 1.3 mmol/g. The hydrodynamic diameter of the bare or PAM-coated primary particles is invariable, ~150 nm, but the size of the aggregates measured under identical kinetic conditions depends on pH and the added amount of PAM. The value of standard deviation is $SD_{(n-1)}$ = 1 for zeta potential, and it varies between 15 and 150 for the hydrodynamic diameter, depending on the mean size. For the sake of clarity, the error bars are omitted.

dx.doi.org/10.1021/la302660p | Langmuir 2012, 28, 16638−16646

extreme values of zeta potential on the left side of Figure 5 and the small values of hydrodynamic diameter in right side of Figure 5. Over the biologically relevant range of pH, the uncoated MNPs are practically unstable even at 0.01 M ionic strength. Adding a small amount of PAM (0.1 mmol/g), the pH of IEP decreases to ∼6 and the pH range of aggregation (the zone of instability) becomes wider. The latter is a known effect of PEs: a small amount of adsorption can destabilize colloidal dispersions due to either bridging particles or forming patch-wise charge heterogeneity on the surface.[40,59,60] Increasing amounts of PAM shift the IEP gradually to more acidic pH (Figure 5, left side) and narrow the pH-range of aggregation (Figure 5, right side). Addition of 1.3 mmol/g of PAM results in stable MNP dispersion at all pH values higher than ∼4. Practically the same behavior was observed in the adsorption of PAA.[35]

Salt Tolerance and Dilution Resistance of Core−Shell MNPs. The salt tolerance of PAM-coated MNPs was characterized by determining the stability ratios (W) at different NaCl concentrations in coagulation kinetics experiments. The stability plots, that is, the changes in the logarithm of the stability ratio (log W) as a function of the logarithm of salt concentration (log c_{NaCl}), can be seen in Figure 6. The salt

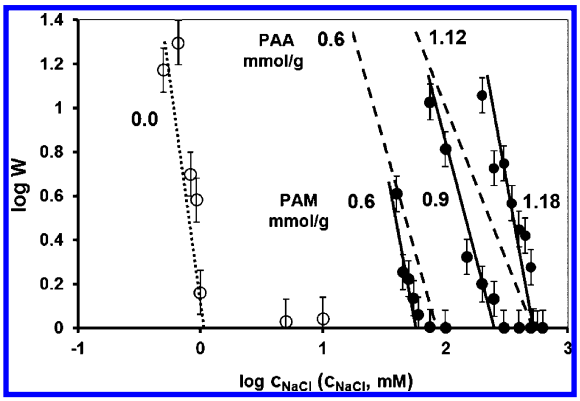

Figure 6. Stability plot to determine the values of the critical coagulation concentration (CCC) of MNPs in the absence of PE coating (open symbols) and in the presence of 0.6, 0.9, and 1.18 mmol/g PAM (filled symbols), measured at pH ≈ 6.5 ($SD_{(n-1)}$ = 0.2; the error bars are omitted for clarity). The previous results of PAA-coated samples[35] (dashed lines) are recalled here for comparison.

tolerance of the MFs is represented by the values of critical coagulation concentration (CCC, the value of c_{NaCl} at log W = 0), characterizing the resistance of the particles against salt-induced aggregation. The dashed lines represent previous results of PAA-coated samples,[35] added here for comparison. The CCC shifts gradually from ∼1 mM for uncoated MNP to ∼60, ∼270, and ∼500 mM at 0.6, 0.9, and 1.18 mmol/g of added PAM, respectively. The resistance against physiological concentration (CCC > 150 mM) is achieved at the PAM addition of ∼0.9 mmol/g, which corresponds to ∼0.8 mmol/g of adsorbed amount, somewhat below the saturation level (0.9 mmol/g). The salt resistance becomes maximal at ∼1.2 mmol/g of added PAM, corresponding to the plateau of the adsorption isotherm (Figure 4). Further increase in the PAM loading to 1.4 and 1.6 mmol/g did not increase the CCC. The value of CCC at the highest achieved salt tolerance was 500 mM in the case of both PAA and PAM, measured at practically the same added amounts of PEs, ∼1.2 mmol/g. The extent of salt resistance cannot be compared to literature results, because there are very few papers[61] publishing coagulation kinetics experiments of polyelectrolyte-coated core/shell MNPs, besides our own publications.[35,40,44] It would be desirable to include such experiments in the processes of premedical qualification of the aqueous magnetic fluids. In the work of Hu and co-workers,[61] it was shown that humate adsorption at pH = 9.8 increased the salt tolerance of MNPs to 125 mM.[61]

The picture is the same in the cases of both PAM and PAA[35] in that saturation of the adsorption layer is sufficient to achieve physiological salt tolerance; however, there are fundamental differences in the stabilizing capabilities of PAM and PAA. First, the log W/log c_{NaCl} slopes of PAA@MNPs are significantly lower than those of PAM@MNPs, the difference being most evident at the highest added amounts of PAA and PAM, 1.12 and 1.18 mmol/g, respectively. This means that PAA@MNP particles are more prone to coagulate at all ionic strengths, as compared to PAM@MNPs. Second, the equilibrium concentrations of the free (nonadsorbed) PEs at the highest salt tolerance are quite different, that is, ∼1 mmol/L for PAM and ∼5 mmol/L for PAA. This shows clearly that magnetite can be stabilized much more efficiently by PAM than by PAA. The third difference is that to attain the value of CCC = 500 mM, an excess of ∼25% of PAA[35] must be added in excess to the amount necessary to reach plateau adsorption (0.6 mmol/g). The excess PAA does not contribute to the adsorption, but remains dissolved in aqueous phase. On the contrary, the same salt tolerance is attained without any excess PAM addition relative to the adsorption plateau. This shows that the coating shell of PAM alone stabilizes the MNPs, while in the case of PAA some additional stabilizing mechanism has to be assumed, which may be connected with the fact that PAA only decorates the surface of MNPs, but does not coat it completely (see the section Electrokinetic Potential, Particle Size, and Aggregation). Because the stabilizing effect of PAA is linked to the presence of nonadsorbed PAA, the MF can lose its colloidal stability, when it becomes diluted during administration. Unbound PEs might also bind and eliminate drugs from the formulations; moreover, their presence could cause adverse effects in biological environments. Thus, it is necessary to minimize the concentration of free PE. Although excess PE can be removed by washing or dialysis,[12] the previously adsorbed PE can also be detached in the process. It is more straightforward to define the appropriate quality and quantity of PE for coating by studying the mechanism of adsorption in similar ways as presented here. It is also worthwhile to note that the same values obtained for hydrodynamic diameter, electrokinetic potential, and CCC values of both PAA@MNPs and PAM@MNPs imply the same quality of coating, and only the adsorption isotherm measurements and their detailed comparative analysis show clearly the advantages of PAM over PAA as coating shell molecule for magnetite nanoparticles.

The dilution resistance of PAM@MNPs was tested to evaluate the stability of the adsorbed PAM layer. The results are presented in Figure 7. In the case of all dispersions, the PAM concentration in the liquid phase decreased to one-half of the equilibrium concentration before dilution (within experimental error), while the adsorbed amount did not change in principle. The PAM@MNP dispersions remained stable after dilution, indicating that unbound PAM could be removed safely from the medium. This behavior is a consequence of the high affinity adsorption of PAM on MNPs (Figure 2) due to the formation

dx.doi.org/10.1021/la302660p | Langmuir 2012, 28, 16638−16646

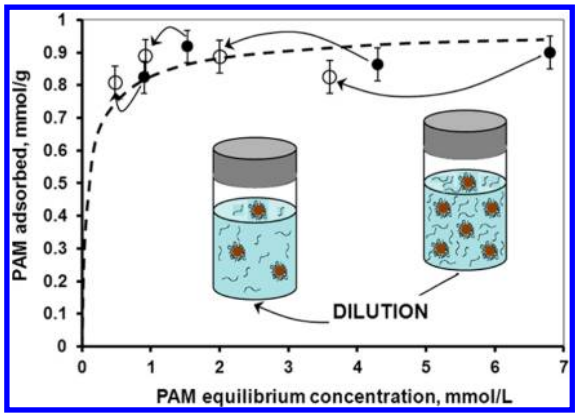

Figure 7. Testing dilution resistance of PAM coating on MNPs. The adsorbed amounts of PAM before (filled symbols) and after (open symbols) dilution are plotted as a function of equilibrium concentration ($SD_{(n-1)}$ = 0.12). The adsorption isotherm (dashed line) and a cartoon of double dilution are inserted for the sake of better understanding.

of direct metal−carboxylate complexes as proved by FTIR-ATR spectra (Figure 3).

As it is also stressed by Jain and co-workers,[28] polymers and polyelectrolytes do not always bind sufficiently strongly; therefore, they can get desorbed (or displaced by other solutes), thus compromising long-term stability of MFs. The methodology we have shown here can be applied generally to investigate the strength of binding of other PEs as well to magnetite or other metal oxide surfaces.

We have tested additionally the time-dependence of the colloidal stability of PAM@MNP prepared with 1.3 mmol/g of added PAM. DLS measurements after storage at +4 °C for 30 and 60 days showed no change in the mean value of Z_{ave} particle size. Insignificant sedimentation was observed at the bottom of the container, but ultrasound agitation prior to DLS measurements (similarly to the experiments with as-prepared samples) fully recovered the original degree of dispersion.

Biocompatibility of PAM@MNP. The results of the blood sedimentation experiments are seen in Table 1 and on the left side of Figure 8. The ESR values practically did not change (Table 1), revealing that the coagulation mechanism of the RBCs was not appreciably influenced by the addition of PAM@MNPs. The homogeneous distribution of the MNPs in the plasma is seen on the left side of Figure 8 as the gradual darkening with increasing magnetite concentration. The picture was taken of samples collected from donor no. 2 right after the ESR measurements; the time span from the mixing with MNPs was approximately 1 h. Darkening of the supernatant plasma makes the ESR results meaningless at higher magnetite concentrations, because of the vanishing optical contrast. However, visual observation proves that BRCs do not coagulate, for example, at 0.32 mg/mL magnetite content (left side of Figure 8). Blood coagulation experiments have also been conducted by Liu and co-workers[62] (using dextran-coated MNPs), and they found the same level of resistance against similar magnetite concentrations as in our experiments.

Table 1. ESR Results of the Blood Samples of the Three Healthy Donors: Loaded with PAM@MNP Dispersion of Different Iron Concentrations and Reference Samples[a]

	ESR (mm/h)		
iron content (mg/mL)	donor no. 1	donor no. 2	donor no. 3
0 (reference sample)[b]	4	10	14
0.024	3	14	15
0.048	3	14	14
0.12	3	15	15

[a]The iron contents in the table are the final concentrations in the blood. [b]Diluted with NaCl solution to the same extent as the MNP-loaded samples.

The results of the cytotoxicity tests show that PAM@MNPs exerted no substantial action on the growth of cancer cells even at the highest concentration, seen on the right side of Figure 8 as the insignificant (less than 6% for each cell lines) extent of proliferation inhibition. The MTT method applied here is widely used for investigation of potential anticancer agents. Because the applied cancer cells exhibit faster cell division, they are more sensitive for antiproliferative intervention than healthy cells. Although the performed MTT assay cannot substitute a comprehensive preclinical toxicological evaluation, it indicates undoubtedly that the PAM@MNP preparation is nontoxic, because cell killing or growth inhibitory action was not detected.

Biocompatibility of the PAM-coated MNPs proved to be similar or even slightly better than that of the PAA-coated ones.[35] While the antiproliferative capacity of PAA@MNPs for two tested cell lines (HeLa and MRC-5) increased to 10−20%, for PAM@MNPs, values higher than 6% have not been observed.

■ CONCLUSIONS

We have presented here an interesting example of the importance of the geometric arrangement of chemically equivalent functional groups in determining the mechanism of polyelectrolyte adsorption. The choice of either PAA or PAM for designing carboxylated coating on MNPs led to the finding that geometric matching between the functional groups of PEs and the surface sites of crystalline phase is at least as important as their chemical affinity. Our results provide indisputable evidence that although the chemical structures of PAA and PAM are nearly identical, both are short-chain linear PEs (1800 and 3000 Da, respectively) with carboxyl moieties, their adsorption features are obviously different. The adsorption of PAA is characterized by H-bonding, a Langmuir-shaped isotherm, and a high concentration of unbound PE, while the much stronger fastening of PAM involves the Fe−carboxylate complex formation leading in turn to high-affinity adsorption (H-type isotherm) and low concentration of free PE in solution. The strong coordinative bonds form at the ≡Fe−OH sites via exchanging the −OH ligands for carboxylates. The PAM@MNPs are not only stable against aggregation, but also resist dilution even under physiological conditions. Because the MFs are ultimately diluted during medical application, this dilution-resistant adsorbed layer makes PAM a superior candidate for core−shell magnetite nanoparticle preparation as compared to PAA. We can conclude that a small difference in the geometric arrangement of carboxylate moieties (in the PAM and PAA chains in this case) alters fundamentally the applicability of carboxylic polyelectrolytes for preparing high-stability core−shell nanoparticles in biocompatible magnetic fluids.

dx.doi.org/10.1021/la302660p | Langmuir 2012, 28, 16638−16646

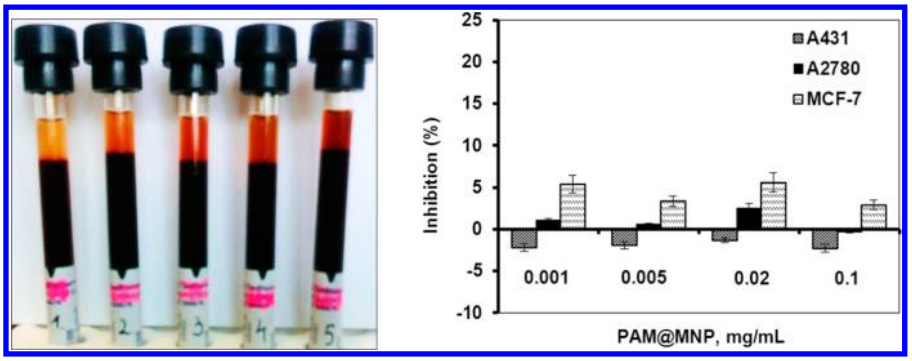

Figure 8. Blood sedimentation experiment (left side): blood sample of donor no. 2 with increasing amounts of added PAM@MNP, from 0 to 0.033, 0.066, 0.16, and 0.32 mg/mL magnetite concentrations, corresponding to vacutainers 1, 2, 3, 4, and 5, respectively. Cytotoxicity experiments (right side): growth inhibition capacity of PAM@MNP on three selected cell lines A431, A2780, and MCF-7. The error bars represent SD with $n = 5$ (five parallel measurements at each PAM@MNP concentration).

AUTHOR INFORMATION

Corresponding Author

*E-mail: tombacz@chem.u-szeged.hu (E.T.), szekeres@chem.u-szeged.hu (M.S.).

Present Address

[§]Semmelweis University, Department of Biophysics and Radiation Biology, Laboratory of Nanochemistry, H-1089 Budapest, Nagyvárad tér 4, Hungary.

Notes

The authors declare no competing financial interest.

ACKNOWLEDGMENTS

This work was supported by the OTKA Foundation (NK84014) and by the Chemistry Doctoral School of University of Szeged. We thank Erika Seres and Katalin Farkas for the blood sedimentation tests performed at the Albert Szent-Gyorgyi Clinical Center (Department of Laboratory Medicine) of the University of Szeged.

REFERENCES

(1) Laurent, S.; Dutz, S.; Häfeli, U. O.; Mahmoudi, M. Magnetic fluid hyperthermia: Focus on superparamagnetic iron oxide nanoparticles. *Adv. Colloid Interface Sci.* **2011**, *166*, 8−23.

(2) Arsalani, N.; Fattahi, H.; Nazarpoor, M. Synthesis and characterization of PVP-functionalized superparamagnetic Fe_3O_4 nanoparticles as an MRI contrast agent. *eXPRESS Polym. Lett.* **2010**, *4*, 329−338.

(3) Janib, S. M.; Moses, A. S.; MacKay, J. A. Imaging and drug delivery using theranostic nanoparticles. *Adv. Drug Delivery Rev.* **2010**, *62*, 1052−1063.

(4) Matthews, S. E.; Pouton, C. W.; Threadgill, M. D. Macromolecular systems for chemotherapy and magnetic resonance imaging. *Adv. Drug Delivery Rev.* **1996**, *18*, 219−267.

(5) Veiseh, O.; Gunn, J. W.; Zhang, M. Design and fabrication of magnetic nanoparticles for targeted drugdelivery and imaging. *Adv. Drug Delivery Rev.* **2010**, *62*, 284−304.

(6) Ma, Y.-H.; Wu, S.-Y.; Wu, T.; Chang, Y.-J.; Hua, M.-Y.; Chen, J.-P. Magnetically targeted thrombolysis with recombinant tissue plasminogen activator bound to polyacrylic acid-coated nanoparticles. *Biomaterials* **2009**, *30*, 3343−3351.

(7) Mishra, B.; Patel, B. B.; Tiwari, S. Colloidal nanocarriers: a review on formulation technology, types and applications toward targeted drug delivery. *Nanotechnol. Biol. Med.* **2010**, *6*, 9−24.

(8) Mahmoudi, M.; Sant, S.; Wang, B.; Laurent, S.; Sen, T. Superparamagnetic iron oxide nanoparticles (SPIONs): development, surface modification and applications in chemotherapy. *Adv. Drug Delivery Rev.* **2011**, *63*, 24−46.

(9) Neuberger, T.; Schöpf, B.; Hofmann, H.; Hofmann, M.; von Rechenberg, B. Superparamagnetic nanoparticles for biomedical applications: Possibilities and limitations of a new drug delivery system. *J. Magn. Magn. Mater.* **2005**, *293*, 483−496.

(10) Gil, P. R.; Hühn, D.; del Mercato, L. L.; Sasse, D.; Parak, W. J. Nanopharmacy: Inorganic nanoscale devices as vectors and active compounds. *Pharmacol. Res.* **2010**, *62*, 115−125.

(11) Kumar, C. S. S. R.; Mohammad, F. Magnetic nanomaterials for hyperthermia-based therapy and controlled drug delivery. *Adv. Drug Delivery Rev.* **2011**, *63*, 789−808.

(12) Liu, G.; Hong, R. Y.; Guo, L.; Li, Y. G.; Li, H. Z. Preparation, characterization and MRI application of carboxymethyl dextran coated magnetic nanoparticles. *Appl. Surf. Sci.* **2011**, *257*, 6711−6717.

(13) Thorek, D. L. J.; Chen, A. K.; Czupryna, J.; Tsourkas, A. Superparamagnetic iron oxide nanoparticle: Probes for molecular imaging. *Ann. Biomed. Eng.* **2006**, *34*, 23−38.

(14) Wang, Y.-X. J. Superparamagnetic iron oxide based MRI contrast agents: current status of clinical application. *Quant. Imaging Med. Surg.* **2011**, *1*, 5−40.

(15) Schlorf, T.; Meincke, M.; Kossel, E.; Glüer, C.-C.; Jansen, O.; Mentlein, R. Biological properties of iron oxide nanoparticles for cellular and molecular magnetic resonance imaging. *Int. J. Mol. Sci.* **2011**, *12*, 12−23.

(16) Ferreira Soares, D. C.; de Oliveira, M. C.; dos Santos, R. G.; Andrade, M. S.; Vilela, J. M. C.; Cardoso, V. N.; Ramaldes, G. A. Liposomes radiolabeled with ^{159}Gd-DTPA-BMA: Preparation, physicochemical characterization, release profile and in vitro cytotoxic evaluation. *Eur. J. Pharm. Sci.* **2011**, *42*, 462−469.

(17) Heinrich, M. C.; Kuhlmann, M. K.; Kohlbacher, S.; Scheer, M.; Grgic, A.; Heckmann, M. B.; Uder, M. Cytotoxicity of iodinated and gadolinium-based contrast agents in renal tubular cells at angiographic concentrations: In vitro study. *Radiology* **2007**, *242*, 425−434.

(18) Bartolini, M. E.; Pekar, J.; Chettle, D. R.; McNeill, F.; Scott, A.; Sykes, J.; Prato, F. S.; Moran, G. R. An investigation of the toxicity of gadolinium based MRI contrast agents using neutron activation analysis. *Magn. Reson. Imaging* **2003**, *21*, 541−544.

(19) Zachary, R. S.; Kievit, F. M.; Zhang, M. Magnetite nanoparticles for medical MR imaging. *Mater. Today* **2011**, *14*, 330−338.

(20) Vékás, L.; Tombácz, E.; Turcu, R.; Morjan, I.; Avdeev, M. V.; Kraisa-Christoforou, T.; Soculiuc, V. Synthesis of magnetic nanoparticles and magnetic fluids for biomedical applications. In *Else Kröner-Fresenius Symposia, Vol. 2, Nanomedicine − Basic and Clinical Applications in Diagnostic and Therapy*; Pahernik, S., Alexiou, C., Eds.; Krager AG: Basel, 2011; pp 35−52.

(21) Lyklema, J.; Deschênes, L. The first step in layer-by-layer deposition: Electrostatics and/or non-electrostatics? *Adv. Colloid Interface Sci.* **2011**, *168*, 135−148.

(22) Cohen Stuart, M. A. Polyelectrolyte adsorption. *J. Phys. (France)* **1988**, *49*, 1001−1008.

(23) Linse, P. Adsorption of weakly charged polyelectrolytes at oppositely charged surfaces. *Macromolecules* **1996**, *29*, 326−336.
(24) Kumagai, M.; Imai, Y.; Nakamura, T.; Yamasaki, Y.; Sekino, M.; Ueno, S.; Hanaoka, K.; Kikuchi, K.; Nagano, T.; Kaneko, E.; Shimokado, K.; Kataoka, K. Iron hydroxide nanoparticles coated with poly(ethylene glycol)-poly(aspartic acid) block copolymer as novel magnetic resonance contrast agents for *in vivo* cancer imaging. *Colloids Surf., B* **2007**, *56*, 174−181.
(25) Zaman, A. A.; Tsuchiya, R.; Moudgil, B. M. Adsorption of a low-molecular-weight polyacrylic acid on silica, alumina, and kaolin. *J. Colloid Interface Sci.* **2002**, *256*, 73−78.
(26) Vermöhlen, K.; Lewandowski, H.; Narres, H.-D.; Koglin, E. Adsorption of polyacrylic acid on aluminium oxide: DRIFT spectroscopy and ab initio calculations. *Colloids Surf., A* **2000**, *170*, 181−189.
(27) Hu, H.; Saniger, J.; Garcia-Alejandre, J.; Castaño, V. M. Fourier transform infrared spectroscopy studies of the reaction between polyacrylic acid and metal oxides. *Mater. Lett.* **1991**, *12*, 281−285.
(28) Jain, N.; Wang, Y.; Jones, S. K.; Hawkett, B. S.; Warr, G. G. Optimized steric stabilization of aqueous ferrofluids and magnetic nanoparticles. *Langmuir* **2010**, *26*, 4465−4472.
(29) Soenen, S. J.; Nuytten, N.; Himmelreich, U.; De Cuyper, M. Intracellular iron oxide nanoparticle coating stability determines nanoparticle usability and cell functionality. *Drug Discovery Today* **2010**, *15*, 1082.
(30) Barrera, C.; Herrera, A.; Zayas, Y.; Rinaldi, C. Surface modification of magnetite nanoparticles for biomedical applications. *J. Magn. Magn. Mater.* **2009**, *321*, 1397−1399.
(31) Barrera, C.; Herrera, A. P.; Rinaldi, C. Colloidal dispersions of monodisperse magnetite nanoparticles modified with poly(ethylene glycol). *J. Colloid Interface Sci.* **2009**, *329*, 107−113.
(32) Forge, D.; Laurent, S.; Gossuin, Y.; Roch, A.; Vander Elst, L.; Muller, R. N. An original route to stabilize and functionalize magnetite nanoparticles for theranosis applications. *J. Magn. Magn. Mater.* **2011**, *323*, 410−415.
(33) Feng, B.; Hong, R. Y.; Wang, L. S.; Guo, L.; Li, H. Z.; Ding, J.; Zheng, Y.; Wei, D. G. Synthesis of Fe_3O_4/APTES/PEG diacid functionalized magnetic nanoparticles for MR imaging. *Colloids Surf., A* **2008**, *328*, 52−59.
(34) Kaaki, K.; Hervé-Aubert, K.; Chiper, M.; Shkilnyy, A.; Soucé, M.; Benoit, R.; Paillard, A.; Dubois, P.; Saboungi, M.-L.; Chourpa, I. Magnetic nanocarriers of doxorubicin coated with poly(ethylene glycol) and folic acid: Relation between coating structure, surface properties, colloidal stability, and cancer cell targeting. *Langmuir* **2012**, *28*, 1496−1505.
(35) Hajdú, A.; Szekeres, M.; Tóth, I. Y.; Bauer, R. A.; Mihály, J.; Zupkó, I.; Tombácz, E. Enhanced stability of polyacrylate-coated magnetite nanoparticles in biorelevant media. *Colloids Surf., B* **2012**, *94*, 242−249.
(36) Felthouse, T. R.; Burnett, J. C.; Horrell, B.; Mummey, M. J.; Kuo, Y. J. Maleic anhydride, maleic acid, and fumaric acid. In *Kirk-Othmer Encyclopedia of Chemical Technology*, 5th ed.; Kroschwitz, J. I., Seidel, A., Eds.; John Wiley & Sons: Hoboken, NJ, 2007; Vol. *15*, pp 481−523.
(37) Hsiou, Y.; Wang, Y.; Liu, L. K. Structures of tetracarbonyl(2−3-*h*-maleic acid)iron, *cis*-$[Fe(C_4H_4O_4)(CO)_4]$ (1) and tetracarbonyl(2−3-*h*-fumaric acid)iron, trans-$[Fe(C_4H_4O_4)(CO)_4]$ (2). *Acta Crystallogr., Sect. C* **1989**, *45*, 721−724.
(38) Bychkova, S. A.; Katrovtseva, A. V.; Kozlovskii, E. V. The potentiometric study of maleic acid complexation with the alkaline-earth metal ions in aqueous solutions. *Russ. J. Coord. Chem.* **2008**, *34*, 172−174.
(39) Rosenqvist, J.; Axe, K.; Sjöberg, S.; Persson, P. Adsorption of dicarboxylates on nano-sized gibbsite particles: effects of ligand structure on bonding mechanisms. *Colloids Surf., A* **2003**, *220*, 91−104.
(40) Illés, E.; Tombácz, E. The effect of humic acid adsorption on pH-dependent surface charging and aggregation of magnetite nanoparticles. *J. Colloid Interface Sci.* **2006**, *295*, 115−123.
(41) Vékás, L.; Bica, D.; Marinica, O. Magnetic nanofluids stabilized with various chain length surfactants. *Rom. Rep. Phys.* **2006**, *58*, 217−228.
(42) Bica, D.; Vékás, L.; Avdeev, M. V.; Marinica, O.; Socoliuc, V.; Balasoiu, M.; Garamus, V. M. Sterically stabilized water based magnetic fluids: Synthesis, structure and properties. *J. Magn. Magn. Mater.* **2007**, *311*, 17−21.
(43) Szekeres, M.; Tombácz, E. Surface charge characterization of metal oxides by potentiometric acid-base titration, revisited theory and experiment. *Colloids Surf., A* **2012**, *414*, 302−313.
(44) Hajdú, A.; Illés, E.; Tombácz, E.; Borbáth, I. Surface charging, polyanionic coating and colloid stability of magnetite nanoparticles. *Colloids Surf., A* **2009**, *347*, 104−108.
(45) Illés, E.; Tombácz, E. The role of variable surface charge and surface complexation in the adsorption of humic acid on magnetite. *Colloids Surf., A* **2004**, *230*, 99−109.
(46) Hunter, R. J. *Foundations of Colloid Science*; Clarendon Press: Oxford, 1989; Vol. *I*.
(47) Kretzschmar, R.; Holthoff, H.; Sticher, H. Influence of pH and humic acid on coagulation kinetics of kaolinite: A dynamic light scattering study. *J. Colloid Interface Sci.* **1998**, *202*, 95−103.
(48) Tombácz, E.; Szekeres, M. Colloidal behavior of aqueous montmorillonite suspensions: the specific role of pH in the presence of indifferent electrolytes. *Appl. Clay Sci.* **2004**, *27*, 75−94.
(49) Piva, E.; Pajola, R.; Temporin, V.; Mario Plebani, M. A new turbidimetric standard to improve the quality assurance of the erythrocyte sedimentation rate measurement. *Clin. Biochem.* **2007**, *40*, 491−495.
(50) Westergren, A. The technique of the red cell sedimentation reaction. *Am. Rev. Tuberc.* **1926**, *14*, 94−101.
(51) Mosmann, T. Rapid colorimetric assay for cellular growth and survival: application to proliferation and cytotoxicity assays. *J. Immunol. Methods* **1983**, *65*, 55−63.
(52) James, R. O.; Parks, G. A. Characterization of aqueous colloids by their electrical double layer and intrinsic surface chemical properties. In *Surface and Colloid Science*; Matijevic, E., Ed.; Plenum Publishing Corp.: New York, 1982; Vol. *12*, pp 119−215.
(53) Lyklema, J. Fundamentals of colloid and interface science. *Solid-Liqiud Interfaces*; Academic Press: London, 1995; Vol. *II*.
(54) Nigam, S.; Barick, K. C.; Bahadur, D. Development of citrate-stabilized Fe_3O_4 nanoparticles: Conjugation and release of doxorubicin for therapeutic applications. *J. Magn. Magn. Mater.* **2011**, *323*, 237−243.
(55) Todorovsky, D. S.; Dumanova, D. G.; Todorovska, R. V.; Getsova, M. M. Preparation and characterization of yttrium-iron citric acid complexes. *Croat. Chim. Acta* **2002**, *75*, 155−164.
(56) Baigorri, R.; García-Mina, J. M.; González-Gaitano, G. Supramolecular association induced by Fe(III) in low molecular weight sodium polyacrylate. *Colloids Surf., A* **2007**, *292*, 212−216.
(57) Krishnamurti, G. S. R.; Huang, P. M. Inluence of citrate ont he kinetics of Fe(II) oxidation and the formation of iron oxyhydroxides. *Clays Clay Miner.* **1991**, *39*, 28−34.
(58) Li, Y.-S.; Church, J. S.; Woodhead, A. L. Infrared and Raman spectroscopic studies on iron oxide magnetic nano-particles and their surface modifications. *J. Magn. Magn. Mater.* **2012**, *324*, 1543−1550.
(59) Gregory, J. Flocculation by polymers and polyelectrolytes. In *Solid/liquid Dispersions*; Tadros, Th. F., Ed.; Academic Press: London, 1987; pp 163−181.
(60) Borkovec, M.; Papastavrou, G. Interactions between solid surfaces with adsorbed polyelectrolytes of opposite charge. *Curr. Opin. Colloid Interface Sci.* **2008**, *13*, 429−437.
(61) Hu, J.-D.; Zevi, Y.; Kou, X.-M.; Xiao, J.; Wang, X.-J.; Jin, Y. Effect of dissolved organic matter on the stability of magnetite nanoparticles under different pH and ionic strength conditions. *Sci. Total Environ.* **2010**, *408*, 3477−3489.
(62) Liu, G.; Hong, R. Y.; Guo, L.; Liu, G. H.; Feng, B.; Li, Y. G. Exothermic effect of dextrancoated Fe3O4 magnetic fluid and its compatibility with blood. *Colloids Surf., A* **2011**, *380*, 327−333.